Effects of exposure and air annealing on MoO$_x$ thin films

Irfan Irfan
Yongli Gao

Effects of exposure and air annealing on MoO$_x$ thin films

Irfan Irfan[a] and Yongli Gao[a,b]

[a]University of Rochester, Department of Physics and Astronomy, Rochester, New York 14627
ygao@pas.rochester.edu
[b]Central South University, Institute for Super Microstructure and Ultrafast Process (ISMUP),
Changsha, Hunan 410083, China

Abstract. Thermally deposited molybdenum oxide films are investigated with X-ray photo-emission spectroscopy, ultra-violet photoemission spectroscopy and inverse photoemission spectroscopy. The Interface between MoO$_x$ and copper pthalocynine (CuPc) is studied and the previously reported device performance improvement is explained, with the help of interface energy level alignment. The effect of oxygen and air exposure on MoO$_x$ films and growth of gap states with exposures are studied. The surface chemical compositions of MoO$_x$ films, of varying thicknesses from 1 nm to 50 nm, have also been investigated. For all the investigated film thicknesses, the thermally evaporated films are found to be oxygen deficient. It is believed, that the oxygen vacancies can be subdued to a great extent by annealing at elevated temperatures. We annealed the MoO$_x$ thin films in air, at 300 °C for 20 h, and investigated the changes induced by the air annealing. © 2012 Society of Photo-Optical Instrumentation Engineers (SPIE). [DOI: 10.1117/1.JPE.2.021213]

1 Introduction

Organic photovoltaic cells (OPV) have attracted enormous attention due to growing energy requirements of the world and declining fossil resources.[1–6] Recently, a lot of progress has been made in OPV with the highest power conversion efficiency now being 10.6% for tandem OPV.[7–10] Organic light emitting diode (OLED) has also observed a phenomenal advancement.[11–16] Other prominent applications of organic semiconductors include organic thin film transistor (OTFT), and efficient spin-injection in organic materials.[17–20] Many attempts have been made to improve the charge transport and collection at electrodes. Tokito et al. were the first to introduce a thin layer of high work function (WF) transition metal oxides between the conducting indium tin oxide (ITO) and organic semiconductor for efficient OLED devices.[21] The importance of the transition metal oxide insertion layer in OPV was successfully demonstrated by a number of research groups.[22–24] The beneficial nature of MoO$_x$ has been established, however, fundamental questions exist in order for comprehensive understanding and controlled utilization of MoO$_x$ insertion layer with reproducible device performance.

One of the fundamental issues is the growth of gap states observed with increasing air and oxygen exposures on MoO$_x$ films.[25] The correlation of growth of gap states with the exposures may provide a better understanding of the role played by MoO$_x$ inter-layers in improving the device performance. Another fundamental issue is oxygen vacancies in thermally evaporated films from MoO$_3$ powder. The evaporated MoO$_x$ films are observed to be strongly n-type due to the oxygen vacancies ($x < 3$).[26–28] The effect of oxygen vacancies, in the stoichiometric MoO$_3$ film, is similar to electron doping. The difference of stoichiometric MoO$_3$ versus oxygen deficient MoO$_x$ inter-layers in devices has been recently reported.[22] Additionally, it is believed that the oxygen deficiencies can be suppressed, to a great extent, by annealing MoO$_x$ at elevated temperatures.

In this paper, we report our investigation on effects of exposure and air annealing on the MoO_x thin films. Copper pthalocynine (CuPc)/indium tin oxide (ITO) and $CuPc/MoO_x$ interfaces were investigated with ultraviolet photoemission spectroscopy (UPS). We observed the vacuum level shifts along with changes in the highest occupied molecular orbital (HOMO) region, with increasing thickness of CuPc film on ITO and MoO_x/ITO substrates. The mechanism of device improvement is explained with the help of interface energy level alignment. We also studied the effect of oxygen and air exposures on growth of the gap states with the UPS. Evolutions of the gap states, with both the exposures, are observed and discussed. The effects of oxygen and moisture on the MoO_x films are observed to progress in two separate stages.

In addition, thermally evaporated MoO_x films, of thicknesses 1, 2, 5, 10, 30 and 50 nm, are investigated with X-ray photoemission spectroscopy (XPS). We measured the oxygen to molybdenum ratio and found that the thermally evaporated films are oxygen deficient. In an attempt to subdue oxygen deficiencies in the MoO_x films, we annealed the films, at 300 °C for 20 h, and measured oxygen to molybdenum values. Our study demonstrates, that contrary to the prevalent belief, the air annealing is not an efficient process of overcoming the oxygen deficiencies in the MoO_x films.

2 Experiment

The UPS measurements, for the interface formation and the exposure studies, were performed using an ultrahigh vacuum (UHV) VG ESCA Lab system equipped with a He discharge lamp. The UHV system consists of a spectrometer chamber interconnected with an evaporation chamber. The base pressure of the spectrometer chamber is typically 8×10^{-11} torr. The base pressure of the evaporation chamber is typically 1×10^{-6} torr. A precision leak valve is also attached with the evaporation chamber to leak desired gases in the chamber for exposure studies. The UPS spectra were recorded by using unfiltered He I (21.22 eV) as the excitation source with the sample biased at -5.00 V, to observe the low-energy secondary cutoff. The UV light spot size on the sample is about 1 mm in diameter. The typical instrumental resolution for the UPS measurements ranges from 0.03 to 0.1 eV, with the photon energy dispersion of less than 20 meV. Substrates for both studies were cut from a borosilicate glass sheet, from Corning, Inc. NY, coated with a 250 nm thick conducting ITO film with resistivity of 15Ω per square. The thicknesses of thermally evaporated films were monitored by quartz crystal microbalance. All the measurements for the interface studies were performed at room temperature.

XPS spectra were measured with a Surface Science Laboratories' SSX-100 system, equipped with a monochromatic Al anode x-ray gun (Kα 1486.6 eV) having resolution limit of 0.5 eV. The base pressure of the system is 9×10 torr. The spot size of the x-ray was selected to be 600 micron in diameter. A substrate, of dimension 11×22 mm, for the annealing study was cut from a gold coated silicon wafer. 10 nm gold was deposited on the substrate with the deposition rate of $\sim$1 nm in every 90 s. MoO_3 powder was thermally evaporated on the substrate. A metallic mask with a sharp edge attached to a moveable micrometer, was placed about $\sim$2 mm below the substrate to evaporate desired thicknesses of MoO_x in a step-wise fashion on the same substrate. The stepped film eliminates variations associated with the deposition conditions for films on different substrate. The sample was then transferred in to the UHV chamber for XPS analysis. After the XPS analysis of the thermally evaporated MoO_x films of stepped thicknesses, the sample was taken out and annealed in air at 300 °C for 20 h on a hot plate from Corning Inc. The temperature was measured with the help of a thermocouple gauge from Fluke. The sample was then transferred back into the SSX-100 chamber for further XPS analysis.

3 Results and Discussions

3.1 *The Effect of MoO_x Inter-layer Between CuPc and ITO*

3.1.1 *CuPc/ITO interface*

In Fig. 1, the UPS spectra of CuPc films on ITO are presented as a function of the thickness of the CuPc films. All the spectra have been normalized to the same height for visual clarity. In Fig. 1(a)
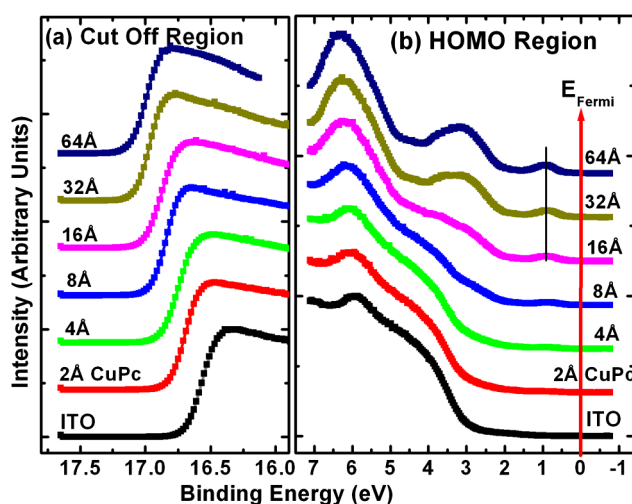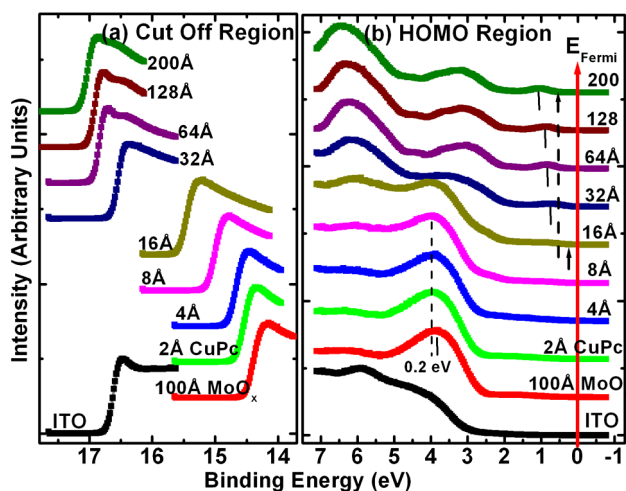
Fig. 1 The UPS spectra of CuPc on ITO as a function of CuPc thickness. The cut-off and the HOMO regions are presented in Fig. 1(a), and 1(b), respectively.

and 1(b), the cut-off and the HOMO regions are presented, respectively. The cut-off binding energy (BE) of the ITO substrate was measured to be 16.57 eV, which corresponds to a surface work function of 4.65 eV, obtained by subtracting the cut-off BE from the photon energy of the excitation source (21.22 eV). With increasing thickness of the CuPc film, we observed cut-off shift towards the lower WF (or higher cut-off BE) values. The shift saturated around 32 Å CuPc thickness. From Fig. 1(b), the HOMO onset for 8 Å CuPc film was measured at 0.31 eV. With further increase in the CuPc thickness, the occupied level peaks remained more or less unchanged on the HOMO peaks, as illustrated by the dashed line in the figure.

3.1.2 CuPc/MoO$_x$ interface

In Fig. 2, the UPS data for the cut-off and the HOMO regions are plotted in Fig. 2(a) and 2(b), respectively. The ITO WF was measured to be 4.59 eV and, with the deposition of a 100 Å MoO$_x$ film, the WF was measured to be 6.82 eV. With the deposition of CuPc on MoO$_x$/ITO, the WF first decreased rapidly, then the shift in WF became more gradual. In Fig. 2(b), the valence band peak of MoO$_x$ was observed at ∼3.8 eV. The MoO$_x$ peak shows a gradual shift towards the higher BE with increasing thickness of CuPc. This shift was measured to be ∼0.2 eV up to

Fig. 2 The UPS spectra of CuPc on MoO$_x$/ITO as a function of CuPc thickness. The cut-off and the HOMO regions are presented in Fig. 1(a) and 1(b), respectively.

8 Å of CuPc deposition. With further CuPc deposition, all the occupied level peaks were observed to be continuously shifting towards the higher BE. The HOMO onset BE for 8 Å, 64 Å, and 200 Å thick CuPc films were measured to be 0.21, 0.36, and 0.53 eV, respectively.
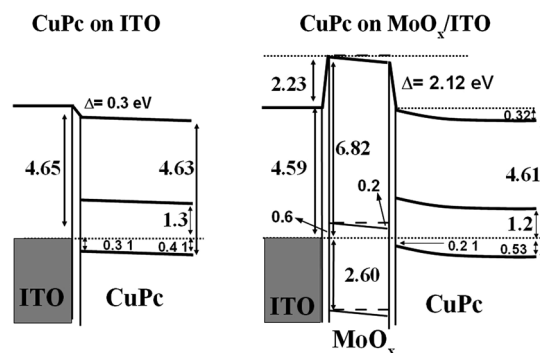
3.1.3 *Energy level alignment*

The energy level alignment diagrams for the CuPc/ITO and the CuPc/MoO$_x$ interfaces are presented in Fig. 3(a) and 3(b), respectively. The band gap of 3.2 eV for MoO$_x$ and 1.7 eV for CuPc hasbeen reported in our earlier works.[26–30] In Fig. 3(a), the ITO WF was measured to be 4.65 eV. At the CuPc/ITO interface, we observed an interface dipole of 0.33 eV, due to transfer of holes from ITO to the CuPc side. After the formation of the interface dipole, a near flat band situation was observed. The initial hole injection barrier was measured to be 0.31 eV, with the ionization potential (IP) of 4.65 eV. In Fig. 3(b), the ITO WF was measured to be 4.59 eV, which became 6.82 eV with the deposition of 100 Å MoO$_x$. With the deposition of CuPc on MoO$_x$/ITO, the energy levels of MoO$_x$ shift towards the higher BE and a large dipole moment at the interface is observed, due to the rapid transfer of holes from MoO$_x$ side to the organic side. The conservative estimate of the shift is 0.2 eV in the MoO$_x$ energy levels towards the higher BE. The estimate is made from the shift of MoO$_x$ valence band peak towards the higher BE with the deposition of CuPc, as depicted in Fig. 2(b). The large interface dipole of 2.97 eV is observed at the interface. The initial hole injection barrier is observed to be 0.21 eV. With further depsition of CuPc, the energy levels gradually relax back to their normal values, thus, creating a band bending like region in the organic side. At the thickness of 200 Å CuPc, the HOMO onset value was measured to be 0.53 eV.

Kim et al. have reported 30 percent improvement in the fill factor (FF) and 37 percent improvement in the overall power conversion efficiency, with a 100 Å MoO$_x$ inter-layer between ITO anode and a CuPc layer.[24] We assign the improvement to the lower hole injection barrier at the CuPc/MoO$_x$ interface and the presence of a drift electric field. There are two possible improvement mechanisms in the presence of the drift electric field. The first is that the drift field is a steering field which is helpful for easier extraction of holes at the anode.[24] The second is that the field facilitates the absorption of photons incident on the material through transparent anode side, which is supported by the reported improved absorption with MoO$_x$ inter-layer.[31]

3.2 *Oxygen and Air Exposure to Molybdenum Oxide Thin Films*

3.2.1 *Evolution of gap states with oxygen exposure*

In our earlier report, we have demonstrated the effect of oxygen exposure on valence band region and WF of MoO$_x$ thin films.[25] High WF (~6.8 eV), of thermally evaporated MoO$_x$ films, decreases sharply with oxygen exposure before reaching a saturation (>5.8 eV). In Fig. 4, the evolution of gap states in the valence band region is presented with increasing oxygen

Fig. 3 The energy level alignment diagrams for, (a) CuPc on ITO, and (b) CuPc on MoO$_x$/ITO interfaces.

exposure on a 50 Å MoO_x film. The spectra of gap states are obtained by subtracting valence region spectrum of evaporated MoO_x film from the background of the valence band region of individual exposed spectrum. Before background subtraction, the dominant oxygen $2p$ peak intensities were normalized and peak position of the evaporated spectrum was shifted to match the peak positions of each of the exposed spectrum. In the figure, we observe the growth of a gap state at <1.0 eV which is marked as 'A'. The gap state is dominant throughout the measurements. Initially, the intensity of the gap state 'A' increases rapidly with the exposures, then it saturates around 10^{10} Langmuir (L) exposure. One Langmuir is equal to the 10^{-6} Torr-sec exposure. In other words, an exposure (in L) can be calculated by multiplying the pressure (in torr) and the duration of the exposure (in seconds) with 10^6. Beyond 10^{10} L exposures, the intensity starts to decrease. A low intensity gap state, around 2.3 eV, is also observed at an early stage of exposure. The intensity of gap state 'B' is observed to be maximum at 10^6 L exposure, and thereafter it starts to diminish. The third gap state, marked as 'C', develops at a mature exposure stage around ∼2.8 eV. At 5×10^{14} L exposure, the intensity of the gap state 'C' is comparable to the gap state 'A'. In the next section, we will discuss the effect of air exposure on MoO_x film.

3.2.2 Evolution of gap states with air exposure

We have reported the effect of air exposures of MoO_x film on the valence region and core levels in our earlier reports.[25,32,33] We have demonstrated that the effect of air exposure on WF is substantial, on the valence band region it is significant, and on the core levels it is almost negligible. The WF decreases sharply with the air exposure before reaching a saturation (>5.4eV). In Fig. 5, the growth of gap states in the valence band region is presented with increasing air exposure on a 50 Å MoO_x film. The presented spectra are obtained by subtracting valence region spectrum of thermally evaporated MoO_x film from a background, as described in Sec. 3.2.1. We observed the growth of a gap state around 1.0 eV, marked as 'D' in the figure, which is similar to the gap state 'A' in Sec. 3.2.1. Initially, the intensity of the state 'D' increases sharply with air exposures, then it saturates around 10^8 L exposure. The gap state 'D' is dominant until 10^{12} L exposure. Another gap state 'E', at ∼2.3 eV, is also observed which is similar to the state 'B' of the previous section. Initially, the intensity of the state 'E' is low. The gap state, marked as 'F', develops at a mature exposure stage around ∼2.9 eV. At the final air exposure, the intensity of the 'F' state is dominant in the spectrum. In the next section, we will compare the evolutions of gap states with the exposures.
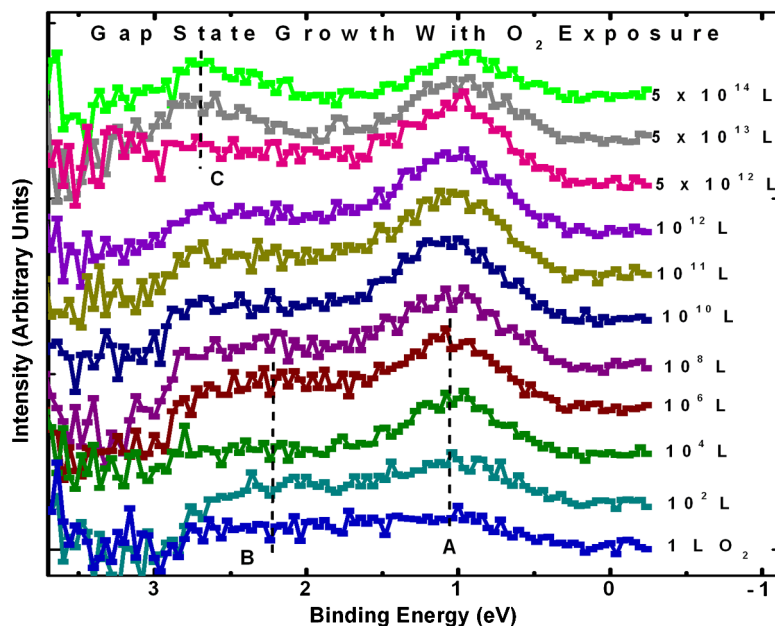

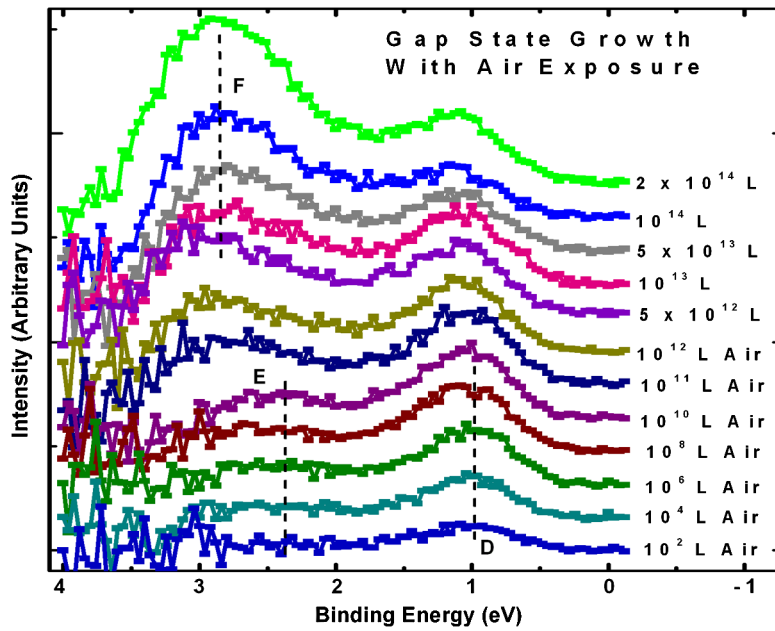**Fig. 4** The evolution of gap states with oxygen exposure.

Fig. 5 The evolution of gap states with air exposure.

3.2.3 *Comparison of growths of gap states*

In Fig. 6, relative intensities of the gap states are presented as a function of the exposures. The intensities of the gap states with the oxygen exposures are presented in Fig. 6(a), and with the air exposures are presented in Fig. 6(b). Comparing the evolution of states 'A' and 'D', both the gap states can be assigned to the effect of oxygen on the MoO_x films. While comparing the evolution of states 'C' and 'F', the origin of these states can be attributed to the effect of moisture on the MoO_x films. Earlier, we have reported that the WF reduction in exposed MoO_x films is a two stage process. The first stage of reduction is caused by adsorption of oxygen on the MoO_x films.[25] This stage reduces the WF from 6.8 to ~5.8 eV. The second stage of WF drop is caused

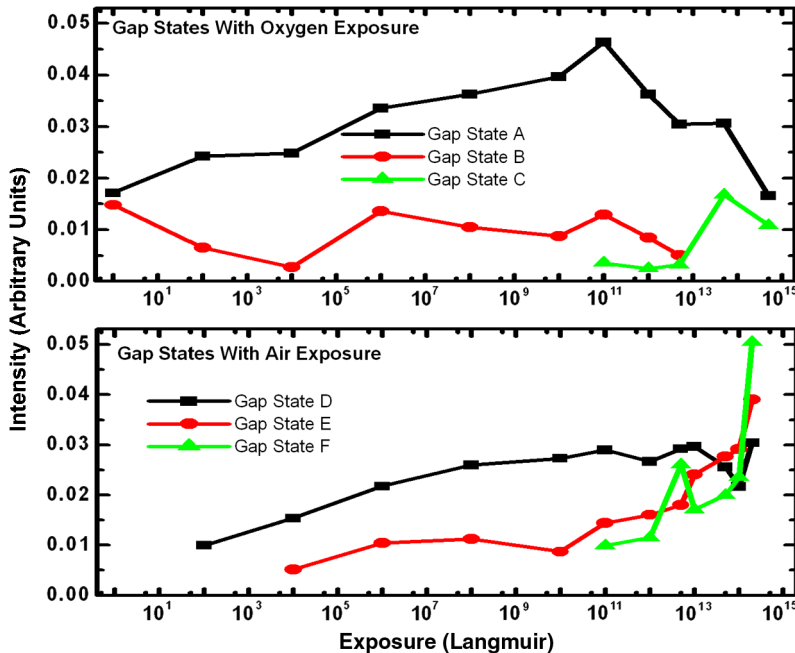**Fig. 6** The comparison of gap states with air and oxygen exposures.

by the adsorption of moisture on the MoO_x films. It is interesting to note, that a gap state similar to the 'A' and the 'D' states, also around 1 eV, has been reported earlier by Nakayama et al. on the initial deposition of MoO_x on poly(dioctylfluorine-alt-benzothiadiazole) (F8BT).[28] Therefore, it can be concluded that the first stage WF drop, caused by oxygen exposure, must be related to the charge transfer between adsorbed oxygen and the surface of MoO_x film.

### 3.2.4 *Correlation of gap states with device performance and work function*

In one of our earlier reports, we have demonstrated a substantial degradation in the device performance with 15 min ($\sim 7 \times 10^{11}$ L) of air exposure of the MoO_x film.[25] The exposures over 10^{11} L also mark the appearance of the gap state 'F' in Fig. 6. Since the growth of the gap state 'F' is caused by moisture, as discussed earlier, we attribute the major degradation in the device to the gap state 'F'. In another report, a similar degradation was observed in the OPV performance by 30 min ($\sim 1.4 \times 10^{12}$ L) of air exposure.[33] It should be noted, that both Nakayama et al.[28] and Maria et al have attributed the improvement of device performance to the presence of the gap state similar to the D state around 1 eV.[29] In our understanding, the WF reduction, from high 6.8 eV to moderate ($\sim$5.8 eV), is coupled with the growth of gap state 'D' (or 'A' for O_2 exposure) and may not be significantly deleterious to devices since the reduced WF is still higher than the ionization potential of most of the organic semiconductors. The appearance of the gap state 'F', which further reduces the WF from $\sim$5.8 to 5.4 eV, is probably the most harmful to devices. Meyer et. al., have also reported no significant effect on the device performance with an air exposure of 3 min (10^{11} L), probably just before the appearance of the gap state F.[34] However, at present, an exact correlation of gap states is not well established and further investigations are required for this to be accomplished.

3.3 *Effect of Annealing on Molybdenum Oxide Thin Films*

In the Sec. 3.1, we reported the beneficial nature of an insertion layer of MoO_x film which is in agreement with many earlier reports.[21–24] In the Sec. 3.2, we established that the performance can be substantially affected by high exposures of MoO_x films. In this section, we will explore another fundamental issue related with the stoichiometry of MoO_x films. The deposition of MoO_x insertion layer is mostly achieved with thermal evaporation of MoO_3 powder. Thermally deposited MoO_x films are known to be oxygen deficient ($x < 3$).[35,36] The oxygen deficiencies are also reported to cause gap states, at $\sim$1.1 eV and 2.3 eV, which can affect the device performance.[29] Some reports suggest that annealing can replenish oxygen deficiencies.[37,38] In this section, we will investigate the stoichimetry of thermally evaporated MoO_x films and explore the effect of air annealing on the stoichiometry.

3.3.1 *Thermally evaporated MoO_x film*

In Fig. 7, the XPS data of Mo $3d_{5/2}$ and O 1s core levels, for 1, 2, 5, 10, 30, and 50 nm thicknesses, are plotted. All the spectra have been normalized to the same height for visual clarity. In Fig. 7(a), the 3d core level of molybdenum consists of two spin orbit interaction split peak, $3d_{5/2}$ and $3d_{5/2}$ with the peak separation of 3.15 eV and the intensity ratio of 3:2. The $3d_{5/2}$ peak, for 1 nm thickness, was observed at the binding energy (BE) of 231.97 eV. With the increasing thickness of MoO_x film, the 3d peaks kept gradually shifting towards the lower BE before reaching a saturation at around 30 nm. The overall peak shift, measured in the range of investigation, was 0.23 eV. The full width at half the maximum height (FWHM) of 3d peaks were measured to be $\sim$1.35 eV. In Fig. 7(b), the oxygen 1s core levels, with a dominant peak at the BE of 529.81 eV and a very low intensity peak around $\sim$530.90 eV, are observed for 1 nm thickness. With increasing thickness of the MoO_x film, the dominant oxygen peak kept gradually shifting towards the lower BE with the saturation setting in around 30 nm. The overall peak shift measured from 1 to 50 nm MoO_x film thickness was 0.26 eV. The FWHM for the dominant peak was $\sim$1.4 eV up to 5 nm, which increased to $\sim$1.55 eV for thicker films. A shift of $\sim$0.2 eV in the MoO_x work function (WF) and the valence band peak towards the lower BE has been reported with increasing film thickness from 2 to 30 nm on indium tin oxide (ITO) substrate (19). The
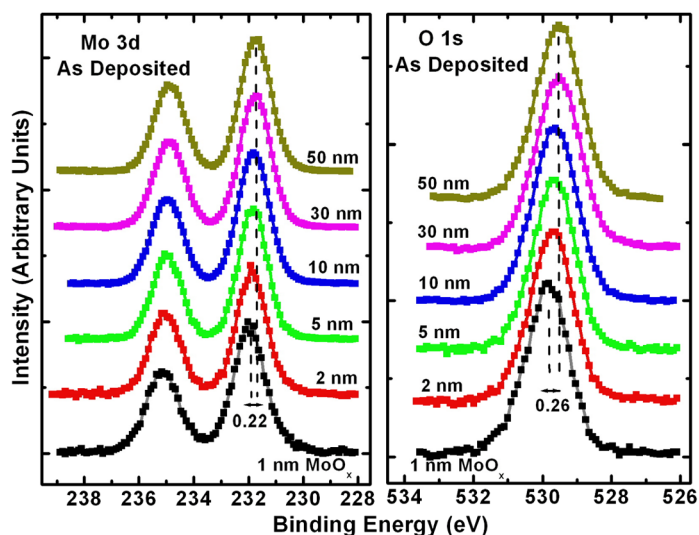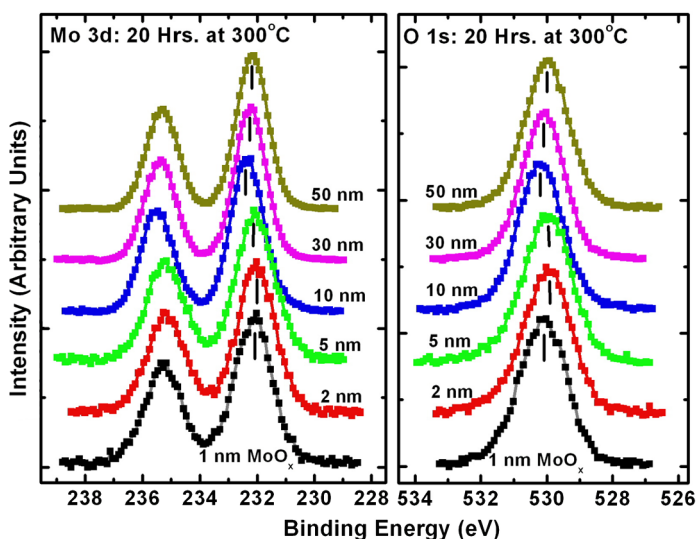
Fig. 7 XPS spectra of (a) Mo 3d, and (b) O 1s core levels as a function of increasing MoO$_x$ film thicknesses.

shift of core levels, observed in the present case, are consistent with the WF shift which further suggests that the shift extend to deep core levels rather than just shallow lying valence band and vacuum level. We also observed Au 4f peaks, originating from substrate, for thin MoO$_x$ depositions up to 5 nmwhich will be discussed later in this work.

3.3.2 Annealing of MoO$_x$ films

In Fig. 8, the XPS data of Mo 3d and O 1s core levels are plotted for 1, 2, 5, 10, 30, 50 nm thicknesses, after annealing in air at 300 °C for 20 h. All the spectra have been normalized to the same height for visual clarity. In Fig. 8(a), the 3d$_{5/2}$ peak for 1 nm thickness was observed at the BE of 231.13 eV. With increasing thickness of MoO$_x$ film, a complex peak shift pattern was observed. We also observed diffusion of gold from substrate towards the top surface through MoO$_x$ film due to annealing for long time at high temperature. The complex peak shift pattern is originated due to diffusion of gold which will be discussed in the next section. The FWHM of 3d peaks was measured to be ~1.35 eV. In Fig. 8(b), the oxygen 1s core level, with a dominant peak


Fig. 8 XPS spectra of (a) Mo 3d, and (b) O 1s core levels after the annealing, as a function of increasing MoO$_x$ film thicknesses.

at the BE of 530.08 eV and a low intensity peak around ~531.44 eV, was observed for 1 nm thickness. The complex peak shift, after annealing, was also present in O 1s core levels with increasing thickness of the MoO_x film.
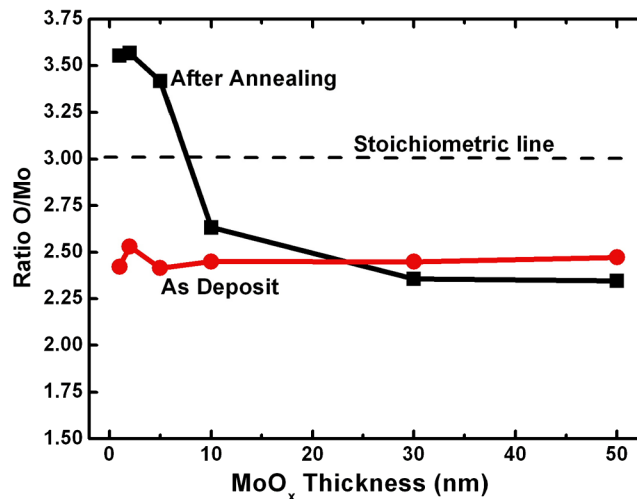
3.3.3 *Comparison of oxygen to molybdenum ratio*

XPS spectra of Au 4f peaks for as deposited and after air annealing are presented in Fig. 9 in order to understand the changes brought in by the annealing. In Fig. 9(a), the 4f core levels of gold consist of two spin orbit interaction split peaks $4f_{7/2}$ and $4f_{5/2}$ with the peak separation of 4.3 eV and the intensity ratio of 4:3. The intensity of 4f peaks kept continuously decreasing and, at 5 nm thickness of MoO_x layer, the intensity of this peak is insignificant. After annealing, the intensity of Au 4f peaks became more than 10 times higher for 1 nm MoO_x thickness, which strongly indicates the diffusion of Au from substrate towards the top surface. With increasing MoO_x thickness, the intensity of Au 4f peaks kept continuously decreasing. The intensity of Au 4f peaks at 10 nm MoO_x thickness, after annealing, is about four times higher that of 1 nm MoO_x for as deposited film. At the 30 nm film thickness, the intensity of Au 4f peaks are low, indicating that the gold diffusion does not significantly affect the surface for such thicknesses. As mentioned earlier in the annealing section, the complex peak shift in the Mo 3d and the O 1s peaks observed after the annealing is most likely originated due to the diffusion of gold.

In Fig. 10, the intensity ratio of oxygen to molybdenum are plotted for 1, 2, 5, 10, 30, and 50 nm thicknesses of MoO_x films before and after the annealing. As obvious from figure, we measured the oxygen to molybdenum ratio about 2.45, with small variation, for deposited film. After annealing, the ratio was initially higher than the stoichiometric value of 3.0 which quickly drops and saturates around ~2.35. Higher value of oxygen to molybdenum ratio, up to 10 nm, is due to higher oxygen content at these thicknesses. As discussed in the previous figure, the annealing of MoO_x thin film with gold substrate causes diffusion of gold atoms towards the surface and substantially enhances the contribution of gold in the surface chemical composition. The contribution becomes insignificant for the 30 nm thick film. Chemisorption of oxygen molecules on gold at high temperature has been reported earlier.[39] Therefore, the enhancement of oxygen intensity for the air annealed MoO_x film at the early stage is due to the chemisorption of oxygen on the diffused gold atoms. Since we do not have significant diffusion of gold on surface (or sub surface) for thicknesses ≥30 nm, the contribution from the chemisorbed oxygen on gold is insignificant. The measured oxygen to molybdenum ratio, in the saturated thickness region, is slightly less (~2.35) for the annealed MoO_x film than the as deposit film (~2.45). Thus, the current investigation establishes that the air annealing does not significantly suppress oxygen vacancies present in the thermally evaporated MoO_x films.
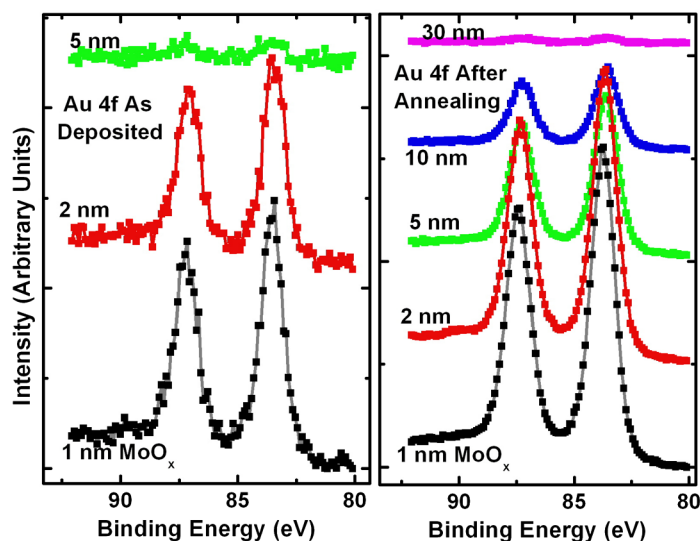
Fig. 9 XPS spectra of Au 4f for (a) a deposit, and (b) after annealing. After annealing intensity of Au 4f peaks increased, indicating diffusion of gold from substrate towards the top surface.

Fig. 10 Oxygen to molybdenum ratio for as deposited and air annealed film with increasing thickness of MoOₓ film. High ratio after the annealing for thin MoOₓ film is due to the absorption of oxygen and moisture on diffused gold atoms.

4 Conclusions

In conclusion, we have investigated the effect of MoO_x inter-layer between ITO anode and CuPc. In the presence of MoO_x, energy levels of organic side are strongly pulled upwards due to high workfunction of MoO_x films, therefore, reducing the hole injection barrier at the interface. The energy levels of organic side gradually relax, therefore, creating a band bending like situatio, which creates a drift electric field. The reduced hole injection barrier and the drift electric field is beneficial for the performance of OLED and OPV devices. Additionally, we have investigated thermally evaporated 1, 2, 5, 10, 30, and 50 nm thick MoO_x films and measured oxygen to molybdenum ratio for these thicknesses. All the films were found to be oxygen deficient ($x < 3$). We performed air annealing of MoO_x films, in air at 300 °C for 20 h, and established that the annealing does not assist in reducing the oxygen vacancies.

Acknowledgments

References

1. C. W. Tang, "Two-layer organic photovoltaic cell," *Appl. Phys. Lett.* **48**(2), 183–185 (1986), http://dx.doi.org/10.1063/1.96937.
2. G. Yu et al., "Polymer photovoltaic cells: enhanced efficiencies via a network of internal donor-acceptor heterojunctions," *Science* **270**(5423), 1789–1791 (1995), http://dx.doi.org/10.1126/science.270.5243.1789.
3. P. Peumans and S. R. Forrest, "Very-high-efficiency double-heterostructure copper phthalocyanine/C-60 photovoltaic cells," *Appl. Phys. Lett.* **79**(1), 126–128 (2001), http://dx.doi.org/10.1063/1.1384001.
4. J. Xue et al., "4.2% efficient organic photovoltaic cells with low series resistances," *Appl. Phys. Lett.* **84**(16), 3013–3015 (2004), http://dx.doi.org/10.1063/1.1713036.
5. G. Li et al., "High-efficiency solution processable polymer photovoltaic cells by self-organization of polymer blends," *Nat. Mater.* **4**(11), 864–868 (2005), http://dx.doi.org/10.1038/nmat1500.
6. C. J. Brabec, "Organic photovoltaics: technology and market," *Sol. Energy Mater. Sol. Cells* **83**(2–3), 273–292 (2004), http://dx.doi.org/10.1016/j.solmat.2004.02.030

7. Y. Sun et al., "Solution-processed small-molecule solar cells with 6.7% efficiency," *Nat. Mater.* **11**(1), 44–48 (2012), http://dx.doi.org/10.1038/nmat3160.

8. C. E. Small and F. So, "High-efficiency inverted dithienogermole-thienopyrrolodione-based polymer solar cells," *Nat. Photonics* **6**(2), 115–120 (2012), http://dx.doi.org/10.1038/nphoton.2011.317.

9. G. Li, R. Zhu, and Y. Yang, "Polymer solar cells," *Nat. Photonics* **6**(3), 153–161 (2012), http://dx.doi.org/10.1038/nphoton.2012.11.

10. National Renewable Energy Laboratory (NREL) www.nrel.gov/ncpv/images/efficiency_chart.jpg.

11. C. W. Tang and S. A. Vanslyke, "Organic electroluminescent diodes," *Appl. Phys. Lett.* **51**(12), 913–915 (1987), http://dx.doi.org/10.1063/1.98799.

12. R. H. Friend et al., "Electroluminescence in conjugated polymers," *Nature* **397**(67), 121–128 (1999), http://dx.doi.org/10.1038/16393.

13. S. J. Su et al., "Highly efficient organic blue-and white-light-emitting devices having a carrier- and exciton-confining structure for reduced efficiency roll-off," *Adv. Mater.* **20**(21), 4189–4194 (2008), http://dx.doi.org/10.1002/adma.200801375.

14. M. G. Helander et al., "Chlorinated indium tin oxide electrodes with high work function for organic device compatibility," *Science* **332**(6032), 944–947 (2011), http://dx.doi.org/10.1126/science.1202992.

15. Z. B. Wang et al., "Unlocking the full potential of organic light-emitting diodes on flexible plastic," *Nat. Photonics* **5**(12), 753–757 (2011), http://dx.doi.org/10.1038/nphoton.2011.259.

16. T. H. Han et al., "Extremely efficient flexible organic light-emitting diodes with modified graphene anode," *Nat. Photonics* **6**, 105–110 (2012), http://dx.doi.org/10.1038/nphoton.2011.318.

17. G. Horowitz, "Organic field-effect transistors," *Adv. Mater.* **10**(5), 365–377(1998), http://dx.doi.org/10.1002/(ISSN)1521-4095.

18. C. D. Dimitrakopoulos and D. J. Mascaro, "Organic thin-film transistors: A review of recent advances," *IBM J.Res. Dev.* **45**(1), 11–27 (2001), http://dx.doi.org/10.1147/rd.451.0011.

19. Z. H. Xiong et al., "Giant magnetoresistance in organic spin-valves," *Nature* **427**(6977), 821–824 (2004), http://dx.doi.org/10.1038/nature02325.

20. M. Cinchetti et al., "Determination of spin injection and transport in a ferromagnet/organic semiconductor heterojunction by two-photon photoemission," *Nat. Mater.* **8**(2), 115–119 (2009), http://dx.doi.org/10.1038/nmat2334.

21. S. Tokito, K. Noda, and Y. Taga, "Metal oxides as a hole-injecting layer for an organic electroluminescent device," *J. Phys. D-Appl. Phys.* **29**(11), 2750–2753 (1996), http://dx.doi.org/10.1088/0022-3727/29/11/004.

22. V. Shrotriya et al., "Transition metal oxides as the buffer layer for polymer photovoltaic cells," *Appl. Phys. Lett.* **88**(7), 073508–073510 (2006), http://dx.doi.org/10.1063/1.2174093.

23. M. D. Irwin et al., "p-Type semiconducting nickel oxide as an efficiency-enhancing anode interfacial layer in polymer bulk-heterojunction solar cells," *PNAS* **105**(8), 2783–2787 (2008), http://dx.doi.org/10.1073/pnas.0711990105.

24. D. Y. Kim et al., "The effect of molybdenum oxide interlayer on organic photovoltaic cells," *Appl. Phys. Lett.* **95**(9), 093304–093306 (2009), http://dx.doi.org/10.1063/1.3220064.

25. Irfan H. Ding et al., "Energy level evolution of air and oxygen exposed molybdenum trioxide films," *Appl. Phys. Lett.* **96**(24), 243307–243310 (2010), http://dx.doi.org/10.1063/1.3454779.

26. Irfan H. Ding et al., "Energy level evolution of molybdenum trioxide interlayer between indium tin oxide and organic semiconductor," *Appl. Phys. Lett.* **96**(7), 073304–073306 (2010), http://dx.doi.org/10.1063/1.3309600.

27. M. Kroger et al., "P-type doping of organic wide band gap materials by transition metal oxides: A case-study on Molybdenum trioxide," *Org. Electron* **10**(5), 932–938 (2009), http://dx.doi.org/10.1016/j.orgel.2009.05.007.

28. Y. Nakayama et al., "Origins of improved hole-injection efficiency by the deposition of MoO(3) on the polymeric semiconductor poly (dioctylfluorene-alt-benzothiadiazole)," *Adv. Funct. Mater.* **19**(23), 3746–3752 (2009), http://dx.doi.org/10.1002/adfm.v19:23.

29. V. Maria et al., "Reduced molybdenum oxide as an efficient electron injection layer in polymer light-emitting diodes," *Appl. Phys. Lett.* **98**(12), 123301 (2010),.http://dx.doi.org/10.1063/1.3557502.

30. L. Yan et al., "Direct observation of fermi-level pinning in Cs-doped CuPc film," *Appl. Phys. Lett.* **79**(25), 4148–4150 (2001), http://dx.doi.org/10.1063/1.1426260.

31. D. Y. Kim, G. Sarasqueta, and Franky So, "SnPc: C(60) bulk heterojunction organic photovoltaic cells with MoO(3) interlayer," *Sol. Ener. Mat. Sol. Cells* **93**(8), 1452–1456 (2009), http://dx.doi.org/10.1016/j.solmat.2009.03.011.

32. Irfan M. Zhang et al., "Strong interface p-doping and band bending in C(60) on MoO(x)," *Org. Electron.* **12**(9), 1588–1593 (2011), http://dx.doi.org/10.1016/j.orgel.2011.06.007.

33. M. Zhang et al., "Organic Schottky barrier photovoltaic cells based on MoO(x)/C(60)," *Appl. Phys. Lett.* **96**(18), 183301–183303 (2010), http://dx.doi.org/10.1063/1.3415497.

34. J. Meyer et al., "Effect of contamination on the electronic structure and hole-injection properties of MoO3/organic semiconductor interfaces," *Appl. Phys. Lett.* **96**(13), 133308–133310 (2010), http://dx.doi.org/10.1063/1.3374333.

35. M. Anwar and C. A. Hogarth, "The correlation of various properties of thin-films of moo3 and of the mixed-oxide systems moo3-in2o3 and moo3-sio," *Mater. J. Sci.* **25**(11), 4918–4928 (1990), http://dx.doi.org/10.1007/BF01129962.

36. T. He and J. Yao, "Photochromism of molybdenum oxide," *Photochem. J. Photobiol. C* **4**(2), 125–143 (2003), http://dx.doi.org/10.1016/S1389-5567(03)00025-X.

37. R. S. Patil, M. D. Uplane, and P. S. Patil, "Electrosynthesis of electrochromic molybdenum oxide thin films with rod-like features," *Int. J. Electrochem. Sci.* **3**(3), 259–265 (2008).

38. V. Bhosle, A. Tiwari, and J. Narayan, "Epitaxial growth and properties of MoOx(2 < x < 2.75) films," *J. Appl. Phys.* **97**(8), 083539–083543 (2005), http://dx.doi.org/10.1063/1.1868852.

39. M. A. Chesters and G. A. Somerjai, "The chemisorption of oxygen, water and selected hydrocarbons on the (111) and stepped gold surfaces," *Surf. Sci.* **52**(1), 21–28 (1975), http://dx.doi.org/10.1016/0039-6028(75)90004-7.

Irfan Irfan is a PhD candidate in the Department of Physics and Astronomy at the University of Rochester under the supervision of Professor Yongli Gao. In 2004, he received a BS from the University of Lucknow. He received his MS in physics in 2006 from S. N. Bose National Institute for basic Sciences, Kolkata, India. He joined the University of Rochester in 2007 and is currently studying electronic structure and energy-level alignment at metallorganic semiconductor, metal/oxide/organic semiconductor interfaces. These studies are helpful in understanding and predicting device performances of OLED and OPV cell. His current work focuses on the role of molybdenum tri-oxide insertion layers at the anode of organic semiconductor devices.

Yongli Gao received his BS in physics from Central-South Institute of Mining and Metallurgy, China in 1981, and PhD in physics from Purdue University in 1986 under the guidance of Professor Ron Reifenberger. From 1986 to 1988, he was a postdoctoral fellow with Professor John Weaver at University of Minnesota. He joined the faculty of the University of Rochester in 1988 and was promoted to associate professor and full professor in physics in 1994 and 1999, respectively. He has published over 200 papers on interface formation in organic semiconductors, ultrafast electronic dynamics in metals, semiconductors, and quantum wells, surface stability and interface formation of high Tc superconductors, low-temperature Schottky barrier formation and dielectric layer formation on III–V semiconductors, surface melting, and mechanisms of x-ray photoelectron and Auger electron diffraction.